MNE 14 (2022) 100112

Contents lists available at ScienceDirect

Micro and Nano Engineering

journal homepage: www.sciencedirect.com/journal/micro-and-nano-engineering

Introducing surface functionality on thermoformed polymeric films

Carlos Sáez-Comet [a], Olga Muntada [b], Achille Francone [c], Nekane Lozano [a,*], Marta Fernandez-Regulez [b], Jordi Puiggali [d], Nikolaos Kehagias [e], Clivia M. Sotomayor Torres [c,f], Francesc Perez-Murano [b,*]

[a] Eurecat. Parc Tecnològic del Vallès, Av. Universitat Autònoma, 23, 08290 Cerdanyola del Vallès, Spain
[b] Instituto de Microelectrónica de Barcelona (IMB-CNM, CSIC). Campus de la Universitat Autònoma de Barcelona, 08193 Bellaterra, Spain
[c] Catalan Institute of Nanoscience and Nanotechnology (ICN2), CSIC and BIST, Campus UAB, Bellaterra, 08193 Barcelona, Spain
[d] Universitat Politécnica de Catalunya, Departament d'Enginyeria Química, Av. Eduard Maristany 16, Barcelona 08019, Spain
[e] NCSR Demokritos, Institute of Nanoscience and Nanotechnology, 15341 Agia Paraskevi, Athens, Greece
[f] Institució Catalana de Recerca i Estudis Avancats (ICREA), 08010 Barcelona, Spain

ARTICLE INFO

Keywords:
Thermoforming
Nanoimprint lithography
Plastic injection molding
Surface functionalization

ABSTRACT

We present a fabrication process for the production of 3-dimensional micro-structured polymeric films. The microstructures are fabricated in a single step using thermal nanoimprint lithography as patterning technique. The micro-structured polymer films are then transformed into a 3D shape by means of a plug-assisted thermoforming process, while keeping the functionality of the micro-patterned areas. The preserved functionality is characterized by water contact angle measurements, while the deformation of the micro-structured topographies due to the thermoforming process is analyzed using confocal microscopy and Digital Image Correlation (DIC) techniques. This combined fabrication process represents a promising solution to complement in-mold decoration approaches, enabling the production of new functional surfaces. As the microstructures are fabricated by means of a mechanical modification of the surface, without the need of chemical treatments or coatings, the presented technique represents a promising, simple and green solution, suitable for the industrial fabrication of 3D nonplanar shaped functional surfaces.

1. Introduction

The industrial interest in micro/nm scale patterning of surfaces is broad due to the wide range of applications. Micro / nano-metric texturing makes it possible to provide surfaces with functional properties, such as, for example, hydrophilicity, hydrophobicity, greater adherence, antibacterial, optical or chromatic effects, among others [1]. Several high accuracy methods to pattern surfaces at the micro and nanoscale have been developed [2,3]. However, a methodology for high volume manufacturing at affordable cost is still missing for many applications, especially to define accurate and deterministic patterns on arbitrary and or curved surfaces. In recent years functional micro- and nano- textured surfaces on 3D formed polymeric films with potential in various applications have been a subject of investigation [4–7]. Among them, micro fluidics [8] and tissue culture [9] are some that attract the most interest. Furthermore, there are other potential applications in other industrial sectors such as the automotive industry (interior parts, optics) [10] as well as home and industrial lighting [11], to mention but a few. In these sectors, a recent manufacturing technology known as in-mold electronics is becoming more and more relevant [12]. In-mold labelling (IML) [13] and in-mold decoration (IMD) [14] processes allow to handle and incorporate decorative 3D formed polymeric films on final injection-molded parts. These manufacturing technologies can be further enhanced by using locally micro- and nano- textured films to obtain local and specific functionalities on the surface of the resulting injection molded parts. Furthermore, the micro- and nano- textured polymeric films can also be used as replication inserts, adequately placed on the injection molds [15].

The most widely extended methods to pattern a surface incorporate a lithography process, which defines the lateral dimensions [16]. The tremendous progress in lithography made over several decades has delivered a robust and reliable technology, covering a wide dimensions range from few nanometers to millimeters. A patterning technique that allows local 3D micro- and nano- structuring of thermoplastic films is

* Corresponding authors.
E-mail addresses: nekane.lozano@eurecat.org (N. Lozano), Francesc.Perez@csic.es (F. Perez-Murano).

https://doi.org/10.1016/j.mne.2022.100112
Received 18 August 2021; Received in revised form 25 January 2022; Accepted 4 February 2022
Available online 7 February 2022

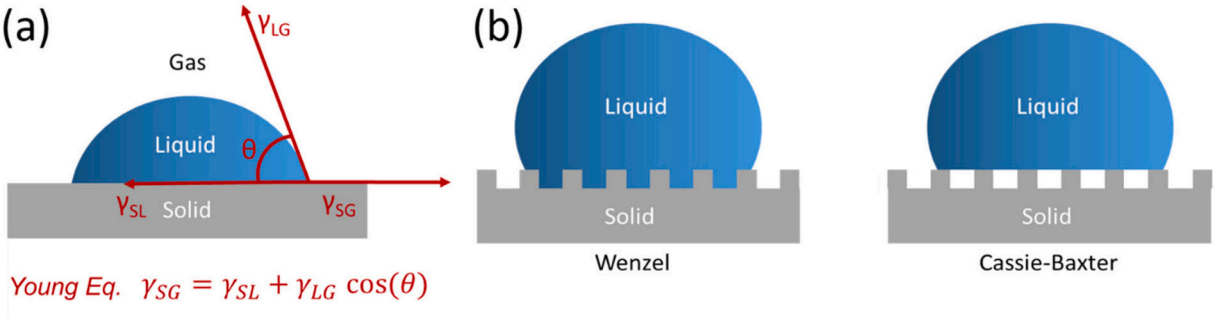

Fig. 1. (a) Graphical representation of the Young equation and contact angle for a droplet on a surface. (b) Graphical representation of the Wenzel and Cassie-Baxter states for a micro-structured surface.

thermal nanoimprint lithography (thermal NIL) [17], a high-resolution and high-throughput lithography technique. Thermal NIL is based on the mechanical deformation of a thermoplastic material, which can be a thermoplastic resist coated on a substrate or a bulk thermoplastic sheet/film, with a stamp containing the surface topography to be replicated in a 1 to 1 scale. The achievable resolution is mainly limited by the minimum feature size that can be fabricated on the stamp and sub-10 nm lateral dimensions have been demonstrated [18]. In order to overcome possible adhesion issues between the stamp and the surface to be patterned, generally an anti-adhesion treatment is applied on the stamp surface [19]. In this work, thermal NIL was used in a step-and-repeat mode, a manufacturing process with potential for high-volume and low-cost manufacturing [20–22]. After imprinting a die, the stamp is released from the substrate, displaced to the next die, put again into contact with the substrate, and thermally imprinted [23].

However, most lithography methods require the printed surface to be flat. Some examples of patterning on curve surfaces exist, like for example in nanostencil lithography [24], but they are not a universal solution and present limited industrial applicability. When it comes to form micro- and nano- textured films into 3D shapes, a well-known and popular transformation process is thermoforming using vacuum-assisted plugs. In this case, the surface is micro-patterned when it is flat, and later it is given the desired final macroscopic shape [25]. Applications of thermoforming in industry are large but so far very few examples of functional patterned thermoformed pieces have been realized [8,9] .

After thermoforming, the patterned areas in the film will suffer geometrical distortions caused by the induced macroscopic deformation. Those distortions might affect negatively the surface functionality. To understand the achievable maximum 3D- macroscale deformations that can be applied to the films without losing the surface functionality, a study of how the macroscopic deformation translates into geometrical distortions at the micro- scale is required. This will then allow to study the loss in the initial surface functionality, if any, and how it could be identified and prevented.

In this article, we present the patterning of polycarbonate (PC) films by thermal-NIL to obtain hydrophobic surfaces. We investigate how their structural and functional properties change when the film is thermoformed. The local changes in the geometries of the various micro-structured zones are monitored using confocal scanning microscopy. The result is compared with to macroscopic deformations and draw ratios obtained by digital image correlation (DIC) [8,26]. A further correlation with surface functionality is carried out by evaluating the wetting behavior of the micro-structured areas of the film before and after the thermoforming process.

2. Pattern and process design

2.1. Pattern design

For investigating the change of the functional properties of a surface submitted to a thermoforming process, we have chosen as test patterns arrays of pillars, because they are relatively simple structures that would allow us to relate the deformation at macroscale due to the thermoforming process with the deformation at the microscale. As a change in the morphology implies a change of the functional properties, we have quantified the variation of the hydrophobicity by measuring the contact angle before and after thermoforming.

Table 1
Calculated values of Wenzel θ_W and Cassie-Baxter contact angles θ_{CB} for the designs of the stamps. A nominal pillar height of 6.5 mm is assumed for all the quadrants.

Quadrant	d (μm)	p (μm)	θ_W	θ_{CB}
Q1	4	8	59°	139°
Q2	6	12	65°	139°
Q3	8	16	68°	139°
Q4	10	20	70°	139°

The hydrophobicity of a surface is commonly defined from the contact angle of a water droplet in contact with the surface as described in the Young's equation [27]:

$$\gamma_{SG} = \gamma_{SL} + \gamma_{LG}\, cos(\theta)$$

Where γ_{SG} is the interfacial tension between solid and gas phases, γ_{SL} between gas and liquid, γ_{LG} between liquid and gas and θ is the angle of a droplet on a solid surface.

To increase the surface contact angle, the interfacial free energy must be increased. This is possible to be achieved by micro-structuring the surface: specific geometries allow air pockets to be trapped between the droplet and the surface. The ideal case where this occurs is known as Cassie-Baxter state and is preferable to the Wenzel state in which the droplet completely wets the surface (Fig. 1.b) [28]. (See Table 1.)

Fig. 2 describes the geometrical parameters of the microstructures that will be transferred to the polycarbonate films, which will induce an increment of the water contact angle. Four designs have been selected, each one consisting of an area of 30 mm × 30 mm covered by pillars with diameters (d) of 4 μm, 6 μm, 8 μm and 10 μm. In each area, the pitch (p) is defined to be 2d. This design will result on four stamps with arrays of holes that, after the thermal-NIL process, will produce pillars in the polycarbonate films.

The Wenzel and Cassie-Baxter water contact angles can be estimated according to the following relations [29]:

$$cos\theta_W = r\cos\theta \quad (1)$$

$$cos\theta_{CB} = \Phi s\,(1+\cos\theta) - 1 \quad (2)$$

where θ_W and θ_{CB} are the apparent contact angle for Wenzel and Cassie-Baxter states respectively, r is the roughness factor, Φs is the area fraction of the solid surface for micro/nanostructured surfaces and θ is the water contact angle on flat –non nanostructured & non-

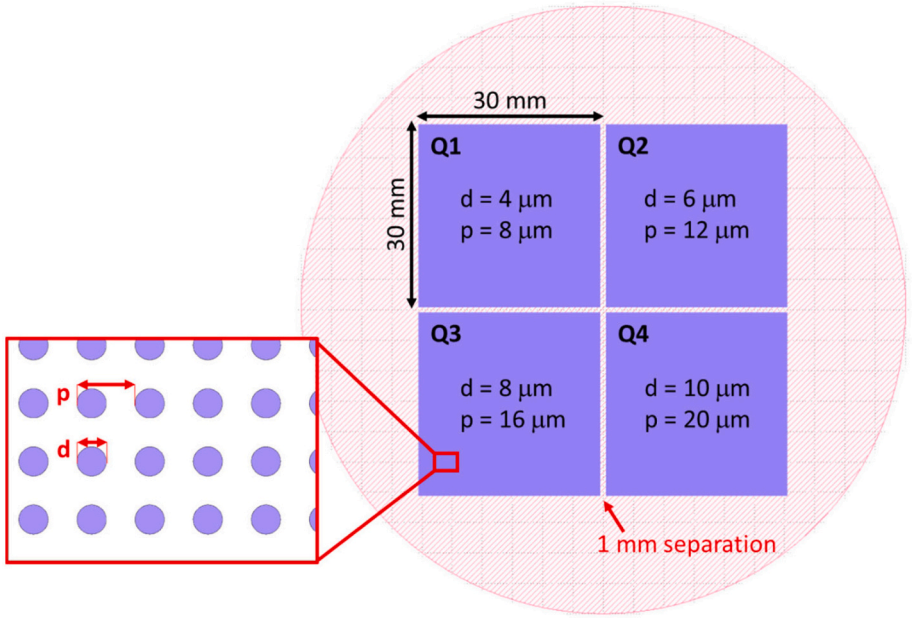

Fig. 2. Micro-structured texture design. The pattern consists of 4 areas of 30 × 30 mm each that contain arrays of holes pillars diameters d ranging from 4 µm to 10 µm and pitches $p = 2d$ for all of them.

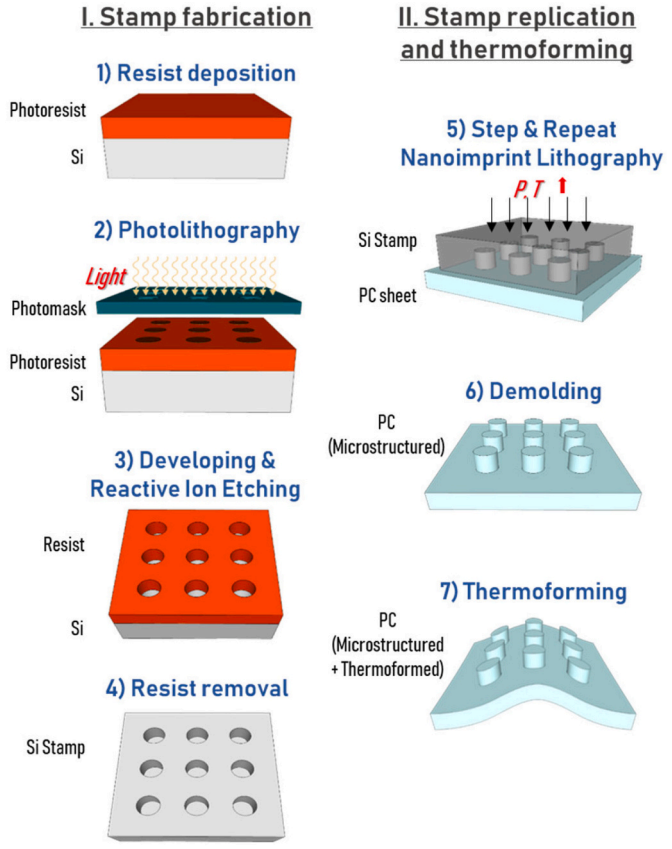

Fig. 3. Scheme of the overall fabrication process which includes the fabrication of the silicon stamp (steps 1–4) the replication of the stamp in a polycarbonate film by thermal NIL (steps 5–6) and the thermoforming of the film (step 7).

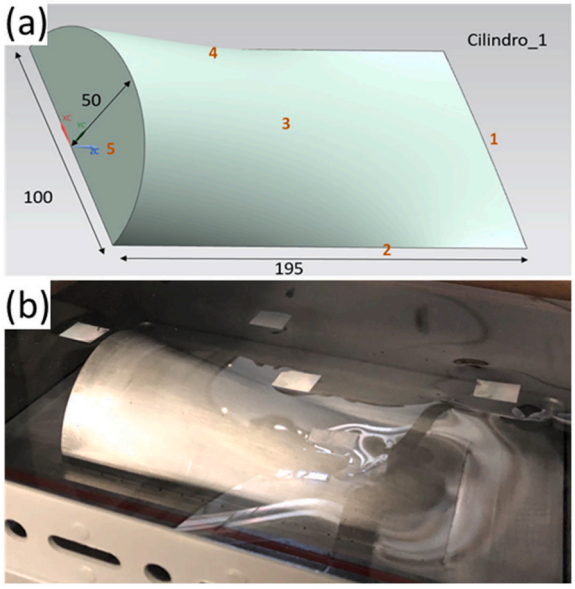

Fig. 4. (a) Design of the thermoforming mold geometry showing the placement of the microstructured areas in red. Dimensions are in millimeters. (b) Photograph of the polycarbonate film on top of the mold prior to the thermoforming process. (For interpretation of the references to colour in this figure legend, the reader is referred to the web version of this article.)

thermoformed PC. r and Φs can be calculated as follows [30]:

$$r = \frac{\left[(p)^2 + \pi dh\right]}{(p)^2} \tag{3}$$

$$\Phi s = \frac{\pi d^2}{4(p)^2} \tag{4}$$

Next table show the values for the expected Wenzel and Cassie-Baxter contact angles for each quadrant of the design, assuming a height of 6.5 µm for the pillars, and a contact angle of 77° for the flat and non- textured surface:

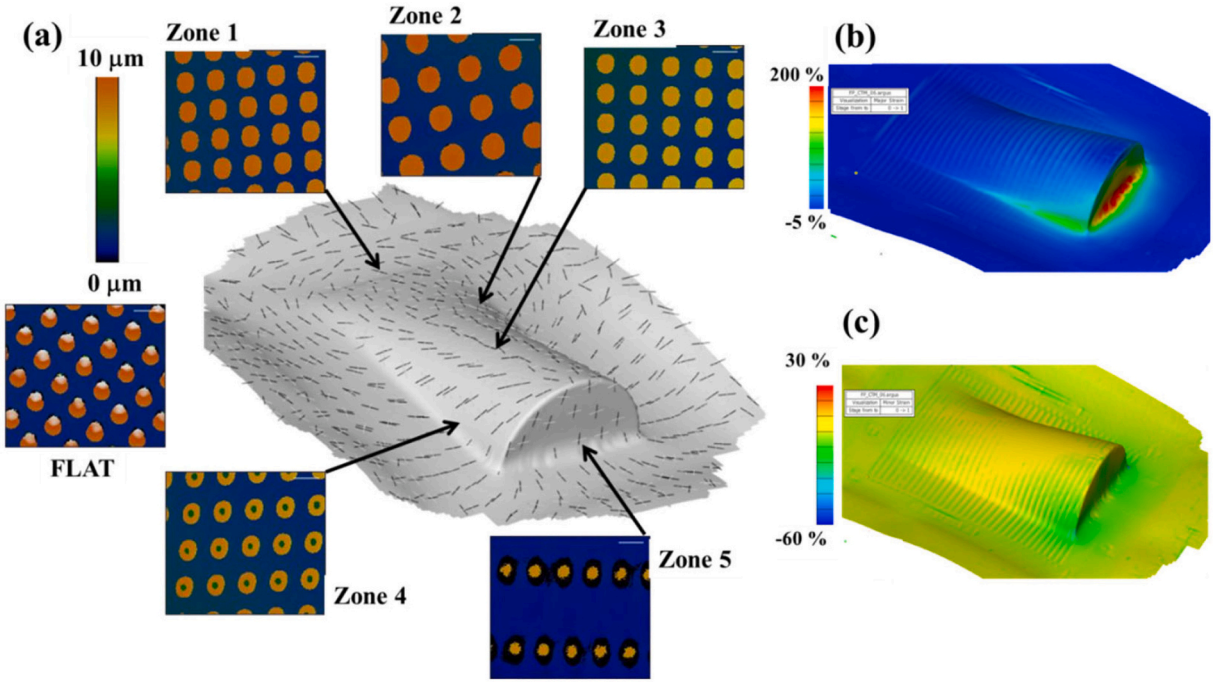

Fig. 5. Detail of the strain in the thermoformed film obtained with the Digital Image Correlation technique. (a): Direction of the major (black lines) and minor (white lines) strain directions. A confocal microscopy image corresponding to each of the imprinted thermal NIL areas illustrates how the microstructure deforms. The values of the major and minor strains at each point of the thermoformed film are represented in Figures (b) and (c), respectively.

Cassie-Baxter states are expected for the textured surfaces, resulting to be more hydrophobic after the patterning process in comparison to the un-patterned ones. Upon deformation, the change of the geometrical parameters of the microstructures will induce a variation in the corresponding water contact angle values, which eventually could imply a deviation from a pure Cassie-Baxter state.

2.2. Process design

The overall process for the fabrication of the thermoformed microstructured film is shown in Fig. 3. The first part of the process is the fabrication of the stamp. Four stamps from the same silicon wafer are fabricated following the designs shown in Fig. 2 by means of optical lithography and reactive ion etching (steps 1–4). After Step 4, the wafer is dived in the four dices, each one containing one of the array designs, which will be used as a master stamp. The master stamp is then pressed and heated against a PC sheet by step and repeat thermal NIL (Step 5). Five micro- structured dies (see Fig. 4.a) of equal dimensions were fabricated in several selected locations of the flat polycarbonate film that was subsequently thermoformed in order to obtain the final 3D shape (see Fig. 4.b). After the demolding (step 6) we obtain a planar micro-structured PC sheet that is thermoformed into a 3D shape using a thermoforming process (step 7). The conditions of these processes are further detailed in the Materials and Methods section.

The geometrical shape chosen for the thermoforming mold is a half-cylinder with decreasing curvature radius, down to 50 mm, a length of 195 mm and a constant width of 100 mm (Fig. 4.a). The placement of the micro-structured zones on the flat film was carefully selected to observe the effects caused by the film deformation in relation to the increasing linear draw ratios and decreasing curvature radii. The mold employed for the thermoforming process, together with the microstructured film on top of it, is shown in Fig. 4.b.

3. Materials and methods

3.1. Silicon stamps fabrication

The first step for the fabrication of the silicon wafers is a 10 min standard cleaning with a piranha solution (H_2SO_4:H_2O_2 2:1) and a rinse with 5% hydrofluoric acid (HF) followed by a photolithography process. The photolithography starts with by spin coating 2 µm of standard positive photoresist HIPR 6512 (Fujifilm) on the wafer, followed by a light exposure through a photomask using a photolithography equipment (Karl Suss MA6 Mask Aligner). Then, the wafer is immersed in OPD 4262 developer (Fujifilm) that dissolves the areas that have been exposed. The remaining photoresist is used as a mask in a modified reactive etching Bosch process (in an Alcatel 601-E equipment) that uses combined pulses of SF_6 as the etching gas and C_4F_8 for the passivation step. The alternation of both gases results in "wells" craved in the silicon with a scalloping contour (Fig. S1 Supplemental). The depth of the wells is designed to be 7 µm for the smallest well. The depth is different for each array as the silicon etching rate depends on the diameter of the wells (Table S1-Supplemental). After the etching process, the remaining resist is stripped from the wafer by means of an oxygen plasma (Power = 600 W; O_2 flow = 600 ml/min; Time = 20 min).

3.2. Thermal NIL patterned films

Transparent 500 µm thick polycarbonate sheets were used as thermoplastic substrates. A NPS 300 stepper (SET) was used as imprinting tool for the step-and-repeat thermal NIL process, using the following process parameters: 190–220 °C as imprinting temperature, 50–80 kg as applied weight, 1–2 min as imprinting time, 60 °C as demolding temperature.

3.3. Thermoforming process

Thermal NIL micro-structured films were thermoformed using a vacuum-assisted aluminum mold with a half-cylinder geometry, as

Table 2
Summary of the characterization results after thermoforming.

	Water contact angle (°)	Standard Deviation (°)	Curvature Radius (mm)	Linear Draw Ratio	AVG major strain (%)	AVG minor strain (%)
Non-textured PC	77.0	±5.3	–	–	–	–
Textured PC (flat)	150.6	±1.6	–	–	–	–
Zone 1	147.7	±4.3	314.5	2.79	2.8	0.3
Zone 2	146	±2.4	211.3	2.98	7.1	1.2
Zone 3	135.9	±8.0	59.8	2.57	11.6	4.6
Zone 4	127.1	±3.1	58.6	2.85	12.1	−1.8
Zone 5	107.1	±5.1	50.1	4.63	97.4	−15.5

shown in Fig. 4 (b), in which the micro-structured zones are pointing outwards. During the thermoforming process, the heating stage parameters were set at 430 °C for 11.5 s (upper heaters) and 500 °C for 12.5 s (lower heaters), and the deformation stage had a duration of 1 s. The mold was kept at 80 °C during the whole cycle and pre-vacuum and vacuum times were set at 4″ and 3″, respectively, using a vacuum power of 15 W (pressure in the circuit 6 bar).

3.4. Structural characterization

The local strains and thickness reductions taking place on the films were assessed using *Digital Image Correlation (DIC)* technique [26], comparing digital images of the same films (taken from exactly the same place) before and after thermoforming. The DIC technique allows the identification of the position of each object point in the two images (before and after thermoforming) by applying a correlation algorithm based on the tracking of the grey value pattern G(x,y) in small local neighbourhood facets. Then, the characterization of local in-plane deformations can be determined by the position of these points. Prior to performing the DIC analysis, a stochastic dot-based intensity pattern was defined on the thermoplastic film's surface via serigraphy and a stereoscopic sensor setup was used for the photographic process.

In addition, the local linear draw ratios, representative of the degree of geometrical deformation and local film stretching of the different micro-structured zones, were determined in order to check the effects on the microstructures produced by varying deformations. Local linear draw ratios are defined as the ratio of the projected length of a line crossing the centre of the thermoformed zone to the length in the unformed sheet and were calculated by DIC for each of the micro-structured zones and for the two orthogonal strain directions (major and minor) as shown in Fig. 5.

3.5. Contact angle characterization

Finally, water contact angle measurements (WCA) of the virgin PC film and the micro-structured zones before and after thermoforming were taken using a tensiometer (Dataphysics OCA 15 CE) and image processing software (SCA 2.0). Micro-droplets of 150 µL of deionized water were used. The contact angle values are obtained as the average of 5 measurements.

4. Results and discussion

The study of the effect of the thermoforming process on the microstructure has been carried out using the stamp with the array Q2 (lateral dimensions $d = 6\ \mu m$ and $p = 12\ \mu m$; Fig. 2) for all the zones depicted in Fig. 4.b except for zone 2, where the array Q3 was used ($d = 8\ \mu m$ and $p = 16\ \mu m$). As both arrays have the same d/p ratio, the theoretical Cassie-Baxter contact angle remains unaffected, and in consequence, this zone is also considered in the analysis.

Before the thermoforming, the five zones were imprinted by thermal NIL and characterized by confocal microscopy in areas of 250 × 190 μm^2. The height of the pillars ranged between 9.4 and 10.4 µm and the pillar diameter resulted to be 6.6 µm ± 0.3 µm. Representative optical and SEM images of the microstructured zones are included in the supplemental information (Figs. S3 and S4). Table 2 summarizes the results of the characterization of the textured PC films for the zones 1 to 5 depicted in Fig. 3.

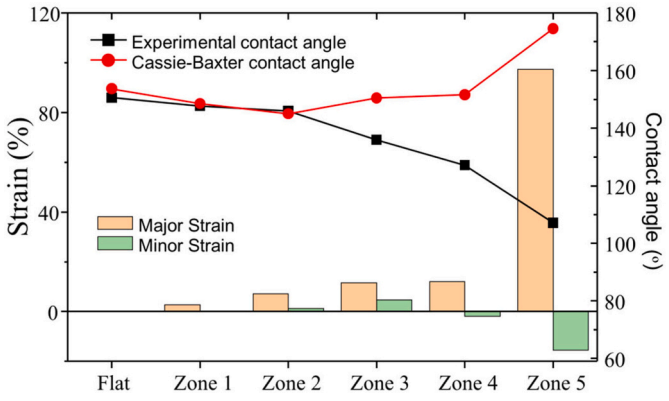

Fig. 6. Chart showing the experimental and theoretical (Cassie-Baxter) contact angles in relation to the local major/minor strains for each of the micro-structured zones considered. To calculate the Cassie-Baxter contact angle, the procedure described in [28] was followed.

In order to determine the wettability behavior for the imprinted areas (prior to thermoforming), the water contact angle was measured, showing an average value of 150.6°. This represents almost a two-fold increase compared to the value of 77° obtained for the non-microstructured PC film. The micro-structuring therefore modifies the surface wetting behavior of the PC, making it superhydrophobic [31]. After thermoforming, the hydrophobic character of the surfaces is preserved even at curvature radius of 50.1 mm and a linear draw ratio of 4.63. The experimental contact angles and the local deformation (strain) observed via the DIC technique are represented in Fig. 6 for each of the five selected zones. The zone that suffered the highest stretching is Zone 5, where the water contact angle value descended to 107.1° compared to the original value before thermoforming (150.6°). This indicates a loss of the hydrophobic character, but still representing an improvement when compared to that of the unformed flat PC film. Representative optical images of the water droplets for measuring the contact angle are displayed in the supplemental information (Fig. S5).

Initially, a theoretical estimation of the water contact angle for the different deformed microstructures after the thermoforming was conducted applying the analytical method described in [30]. In this model, the variation of the contact angle shown by different low aspect ratio pillar geometries (almost barrel-shaped) can be estimated as a function of the nanostructure roughness parameters a, b and h; being a the diameter at the top of the nanopillar, b the distance between the top corners of a pillar and h the height of the nanopillar. In our case, these parameters were carefully extracted from confocal microscopy images of each of the flat and thermoformed nanostructures. However, the images of the confocal microscope show a more elliptical size for the pillars, as well as an asymmetric deformation of the pillar array, in accordance with the difference between major and minor strains. Because of this, we modelled the expected contact angle from the deformed microstructures

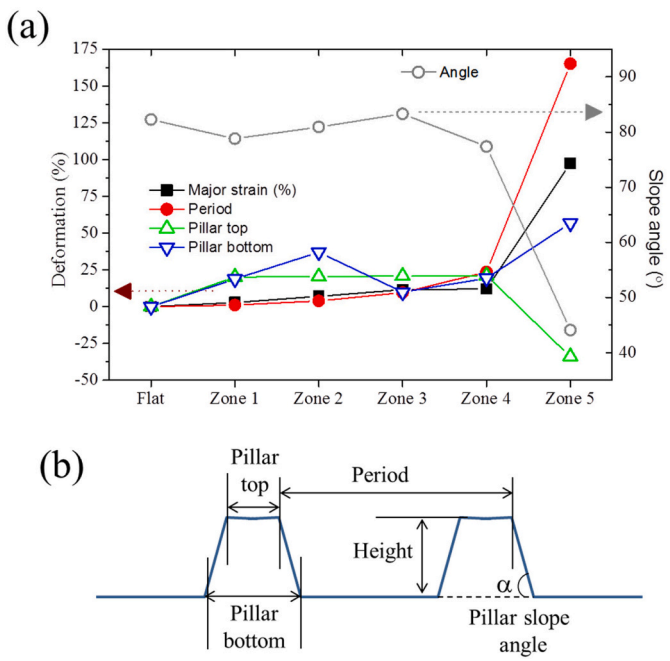

Fig. 7. (a) Geometrical deformation suffered by the pillars at each zone of the thermoformed film. (b) Scheme to refer to each of the geometrical parameters.

following the procedure described in [28], which accounts for an irregular pillar shape (data is shown in the supplemental information). The result is displayed in the red curve of Fig. 6. Even using this second formalism, it is obtained that the Wenzel and Cassie-Baxter contact angle theoretical estimation does not follow the trend determined by the experimental contact angle.

The discrepancy between the experimental contact angle and the contact angle estimation assuming a Cassie-Baxter state can be explain attending to the specific deformation that the microstructures suffer when submitted to deformation. A detailed characterization by confocal microscopy of the pillars after the thermoforming process reveals that the base of the pillar increases significantly with the strain at which the plastic film is submitted to. We have quantified this deformation recording the most significant geometrical parameters, as displayed in Fig. 7, for the direction of major strain (Data is shown numerically in the supplemental information).

It is remarkable that the slope angle of the pillar decreases significantly for the zones 4 and 5, following the same trend than the experimental water contact angle. According to the above observation, we hypothesize that the deformation of the pillars increases the actual surface area that is wet by water. The fact that the pillar slope angle decreases implies that the water wets not only the top of pillar, but it also occupies part of the volume between the pillars. Consequently, the contact angle behavior separates from a pure Cassie-Baxter state and approaches to a Wenzel like state. This observation brings us to conclude that that the macroscopic determination of the strain caused by the thermoforming process is not enough to predict the change of the surface properties when the functionalization is generated by an array of microstructures. It implies that in order to predict the final functional of a textured surface after being submitted to a thermoforming process, the manner that the microstructures deform must be accurately investigated.

5. Conclusions

We have presented the controlled incorporation of hydrophobicity in PC films by a combination of thermal-NIL patterning and thermoforming. An initial super-hydrophobic contact angle of 150° is achieved for the flat micro-structured patches on the films (which represents a two-fold increase with respect to the non-patterned films (77°)). The contact angles of the micro-structured patches after the macroscopic deformations suffered by the film during thermoforming have been measured and correlated with the local major and minor in-plane strains, using the *DIC* technique. For extreme deformations during the thermoforming process, the hydrophobic character decreases but a substantial hydrophobicity is still retained compared to that of the initial non micro-structured film.

An analytical model developed by Zheng and Lü [28] to predict the water contact angle as a function of micro-pillar geometry based on the Cassie-Baxter equation is applied to the particular case of geometrical variations produced by in-plane deformations resulting from the thermoforming process. This prediction seems to work well for most of the thermoforming induced-deformation. However, it deviates for areas were the strain is larger. This deviation might be explained by the fact that, for a very large deformation, either the surface presents a more Wenzel state or the Cassie Baxter modelling does not capture the asymmetric deformation experienced by the pillars.

In conclusion, the methodology we have presented here can be used to predict the change in functional properties of a microtextured surface film when subjected to a thermoforming process. Consequently, it could be used, for example, to define geometric parameters of patterns on the NIL stamps to bestow a given texture to the surface prior to thermoforming, knowing a priori the local deformation each area of the surface will experience. It can also provide clues of which maximum strain a thermoformed film can sustain to retain its functional properties.

Declaration of Competing Interest

The authors declare that they have no known competing financial interests or personal relationships that could have appeared to influence the work reported in this paper.

Acknowledgements

This work has been performed within the PLASTFUN project (*Planta Pilot de Peces Plàstiques amb Superficies Funcionals Avançades*), within the Industries of the Future community (IDF) RIS3CAT, supported by the European Regional Development Fund (ERDF) as part of the operative frame FEDER of Catalonia 2014-2020 EC [COMRDI 16-1-0018], included in the 7th Framework Program. Carlos Sáez also acknowledges the funding received from "Departament d'Economia I Coneixement de la Generalitat de Catalunya" in the frame of the "Doctorats Industrials" program. AF, NK and CMST acknowledge support from the S. Ochoa program from the Spanish Research Agency (AEI, grant no. SEV-2017-0706) and by the CERCA Programme of the Generalitat de Catalunya.

Appendix A. Supplementary data

Supplementary data to this article can be found online at https://doi.org/10.1016/j.mne.2022.100112.

References

[1] K. Ellinas, A. Tserepi, E. Gogolides, Durable superhydrophobic and superamphiphobic polymeric surfaces and their applications: a review, Adv. Colloid Interf. Sci. 250 (2017) 132–157, https://doi.org/10.1016/j.cis.2017.09.003.

[2] E. Gogolides, K. Ellinas, A. Tserepi, Hierarchical micro and nano structured, hydrophilic, superhydrophobic and superoleophobic surfaces incorporated in microfluidics, microarrays and lab on chip microsystems, Microelectron. Eng. 132 (2015) 135–155, https://doi.org/10.1016/J.MEE.2014.10.002.

[3] M. Lohse, M. Heinrich, S. Grützner, A. Haase, I. Ramos, C. Salado, M.W. Thesen, G. Grützner, Versatile fabrication method for multiscale hierarchical structured polymer masters using a combination of photo- and nanoimprint lithography, Micro Nano Eng. 10 (2021), 100079, https://doi.org/10.1016/j.mne.2020.100079.

[4] A. Fernández, A. Francone, L.H. Thamdrup, A. Johansson, B. Bilenberg, T. Nielsen, M. Guttmann, C.M. Sotomayor Torres, N. Kehagias, Hierarchical surfaces for enhanced self-cleaning applications, J. Micromech. Microeng. 27 (2017), 045020, https://doi.org/10.1088/1361-6439/aa62bb.
[5] A. Fernández, A. Francone, L.H. Thamdrup, A. Johansson, B. Bilenberg, T. Nielsen, M. Guttmann, C.M. Sotomayor Torres, N. Kehagias, Design of hierarchical surfaces for tuning wetting characteristics, ACS Appl. Mater. Interfaces 9 (2017) 7701–7709, https://doi.org/10.1021/acsami.6b13615.
[6] A. Perez-Gavilan, J.V. de Castro, A. Arana, S. Merino, A. Retolaza, S.A. Alves, A. Francone, N. Kehagias, C.M. Sotomayor-Torres, D. Cocina, R. Mortera, S. Crapanzano, C.J. Pelegrín, M.C. Garrigos, A. Jiménez, B. Galindo, M.C. Araque, D. Dykeman, N.M. Neves, J.M. Marimón, Antibacterial activity testing methods for hydrophobic patterned surfaces, Sci. Rep. 11 (2021) 6675, https://doi.org/10.1038/s41598-021-85995-9.
[7] N. Kehagias, A. Francone, M. Guttmann, F. Winkler, A. Fernández, C.M. Sotomayor Torres, Fabrication and replication of re-entrant structures by nanoimprint lithography methods, J. Vac. Sci. Technol. B. 36 (2018) 06JF01, https://doi.org/10.1116/1.5048241.
[8] T. Senn, C. Waberski, J. Wolf, J.P. Esquivel, N. Sabaté, B. Löchel, 3D structuring of polymer parts using thermoforming processes, Microelectron. Eng. 88 (2011) 11–16, https://doi.org/10.1016/j.mee.2010.08.003.
[9] S. Giselbrecht, T. Gietzelt, E. Gottwald, C. Trautmann, R. Truckenmüller, K. F. Weibezahn, A. Welle, 3D tissue culture substrates produced by microthermoforming of pre-processed polymer films, Biomed. Microdevices 8 (2006) 191–199, https://doi.org/10.1007/s10544-006-8174-8.
[10] S.-H. Shin, B. Hwang, Z.-J. Zhao, S.H. Jeon, J. Jung, J.-H. Lee, B.-K. Ju, J.-H. Jeong, Transparent displays utilizing nanopatterned quantum dot films, Sci. Rep. 8 (2018) 2463, https://doi.org/10.1038/s41598-018-20869-1.
[11] A. Peter Amalathas, M.M. Alkaisi, Nanostructures for light trapping in thin film solar cells, Micromachines. 10 (2019), https://doi.org/10.3390/mi10090619.
[12] Y. Gong, K.J. Cha, J.M. Park, Deformation characteristics and resistance distribution in thermoforming of printed electrical circuits for in-mold electronics application, Int. J. Adv. Manuf. Technol. 108 (2020) 749–758, https://doi.org/10.1007/s00170-020-05377-9.
[13] S. Chen, S. Zhang, Mechanical Behaviors and Thermoforming Features of PMMA Used In-mold Decoration 500, 2014, pp. 440–443, https://doi.org/10.4028/www.scientific.net/AMM.496-500.440.
[14] S.-C. Chen, S.-T. Huang, M.-C. Lin, R.-D. Chien, Study on the thermoforming of PC films used for in-mold decoration, Int. Commun. Heat Mass Transf. 35 (2008) 967–973, https://doi.org/10.1016/j.icheatmasstransfer.2008.04.008.
[15] O. Muntada-López, J. Pina-Estany, C. Colominas, J. Fraxedas, F. Pérez-Murano, A. García-Granada, Replication of nanoscale surface gratings via injection molding, Micro Nano Eng. 3 (2019) 37–43, https://doi.org/10.1016/J.MNE.2019.03.003.
[16] J.M.D.T. Nogueras, Nanofabrication, IOP Publishing Ltd, 2020, https://doi.org/10.1088/978-0-7503-2608-7.
[17] S.Y. Chou, P.R. Krauss, P.J. Renstrom, Imprint of sub-25 nm vias and trenches in polymers, Appl. Phys. Lett. 67 (1995) 3114, https://doi.org/10.1063/1.114851.
[18] P.R. Krauss, S.Y. Chou, Sub-10 nm imprint lithography and applications, in: Annu. Device Res. Conf. Dig, IEEE, 1997, pp. 90–91, https://doi.org/10.1116/1.589752.
[19] A. Francone, Materials and anti-adhesive issues in UV-NIL. PhD Thesis. Institut National Polytechnique de Grenoble-INPG, 2010.
[20] S.V. Sreenivasan, Nanoimprint lithography steppers for volume fabrication of leading-edge semiconductor integrated circuits, Microsyst. Nanoeng. 3 (2017) 1–19, https://doi.org/10.1038/micronano.2017.75.
[21] M. Otto, Reproducibility and homogeneity in step and repeat UV-nanoimprint lithography, Microelectron. Eng. 73–74 (2004) 152–156, https://doi.org/10.1016/j.mee.2004.02.032.
[22] T. Haatainen, P. Majander, T. Mäkelä, J. Ahopelto, Imprinted 50 nm features by UV step and stamp imprint lithography method, in: Dig. Pap. - Microprocess. Nanotechnol. 2007; 20th Int. Microprocess. Nanotechnol. Conf. MNC, 2007, pp. 280–281, https://doi.org/10.1109/IMNC.2007.4456213.
[23] A. Francone, T. Kehoe, I. Obieta, V. Saez-Martinez, L. Bilbao, A. Khokhar, N. Gadegaard, C. Simao, N. Kehagias, C. Sotomayor Torres, Integrated 3D hydrogel waveguide out-coupler by step-and-repeat thermal nanoimprint lithography: a promising sensor device for water and pH, Sensors. 18 (2018) 3240, https://doi.org/10.3390/s18103240.
[24] O. Vazquez-Mena, L. Gross, S. Xie, L.G. Villanueva, J. Brugger, Resistless nanofabrication by stencil lithography: a review, Microelectron. Eng. 132 (2015) 236–254, https://doi.org/10.1016/j.mee.2014.08.003.
[25] J. Throne. Technology of Thermoforming (eBook) Hanser Publications, (n.d.). https://www.hanserpublications.com/Products/388-technology-of-thermoforming-ebook.aspx (accessed August 16, 2021).
[26] M. Jerabek, Z. Major, R.W. Lang, Strain determination of polymeric materials using digital image correlation, Polym. Test. 29 (2010) 407–416, https://doi.org/10.1016/j.polymertesting.2010.01.005.
[27] B. Thomas Young, An essay on the cohesion of fluids, Philos. Trans. R. Soc. Lond. A 95 (1805) 65–87, https://doi.org/10.1098/rstl.1805.0005.
[28] Q. Zheng, C. Lü, Size effects of surface roughness to superhydrophobicity, in: Procedia IUTAM, Elsevier B.V, 2014, pp. 462–475, https://doi.org/10.1016/j.piutam.2014.01.041.
[29] C.I. Park, H.E. Jeong, S.H. Lee, H.S. Cho, K.Y. Suh, Wetting transition and optimal design for microstructured surfaces with hydrophobic and hydrophilic materials, J. Colloid Interface Sci. 336 (2009) 298–303, https://doi.org/10.1016/j.jcis.2009.04.022.
[30] E. Puukilainen, T. Rasilainen, M. Suvanto, T.A. Pakkanen, Superhydrophobic polyolefin surfaces: controlled micro- and nanostructures, Langmuir. 23 (2007) 7263–7268, https://doi.org/10.1021/la063588h.
[31] X.J. Feng, L. Jiang, Design and creation of superwetting/antiwetting surfaces, Adv. Mater. 18 (2006) 3063–3078, https://doi.org/10.1002/adma.200501961.